Supplementary Information: Symmetry constrained neural networks for detection and localization of damage in metal plates

James Amarel,[1, a)] Christopher Rudolf,[2, b)] Athanasios Iliopoulos,[3] John Michopoulos,[4] and Leslie N. Smith[5]
[1)] *NRC Research Associate, U.S. Naval Research Laboratory, Washington, DC, 20375, USA*
[2)] *Multifunctional Materials Branch, U.S. Naval Research Laboratory, Washington, DC, 20375, USA*
[3)] *Center for Materials Physics and Technology, U.S. Naval Research Laboratory, Washington, DC, 20375, USA*
[4)] *Principal Scientist of Materials Innovation, U.S. Naval Research Laboratory, Washington, DC, 20375, USA*
[5)] *Navy Center for Applied Research in Artificial Intelligence, U.S. Naval Research Laboratory, Washington, DC, 20375, USA*

(Dated: 30 September 2024)

I. MEASURES OF SYSTEM SYMMETRY

One source of symmetry breaking in our system was the result of differences among the transducer generated waves, which exhibited variations in amplitude, phase, and spectra. On comparing the spectral amplitude of source waveforms (see Figure S1), one sees that while each transducer is of a distinguishable character, all generated waves remain within 1.5% of their typical form. We empirically concluded that these variations in the generated waveforms were not a dominant source of difficulty for our models by selectively investigating prediction errors corresponding to signals generated by transducer 3 of spectral amplitude that differed in excess of 1.25% from the mean spectral amplitude.

Contributions to symmetry-breaking in the absence of damage include the influence of material anisotropies on wave propagation. These effects are reflected in the baseline signals $V_{rs}^{(0)}(t)$, which would be invariant under the square group if symmetry was exact. Thus, a measure of the bare equivariance breaking in our system is provided by the normalized distance

$$R^{(0)}(t) = \frac{1}{8}\sum_{g\in G}\frac{\|V^{(0)}(t) - \rho_g V^{(0)}(t)\|}{\|V^{(0)}(t)\|} \tag{S1}$$

where ρ_g is the appropriate matrix representation of an element g in the square group. On averaging over our 6 baseline signals, in addition to neglecting both the diagonals of V_{rs} and times t before the first Lamb wave arrival, we found $R^{(0)} = 0.73 \pm 0.33$ for the time-averaged relative equivariance error values (see Figure S2). Symmetry-violating features in the baseline signals persist even when neglecting both phase and scale differences (see Figure S3).

Visualization of the training input data symmetry breaking can be achieved by considering the normalized distance error field

$$R(\mathbf{x}) = \frac{1}{8}\sum_{g\in G}\frac{\|V(\mathbf{x}) - \rho_g V(\rho_{g^{-1}}\mathbf{x})\|}{\frac{1}{2}(\|V(\mathbf{x})\| + \|V(\rho_{g^{-1}}\mathbf{x})\|)} \tag{S2}$$

with $V(\mathbf{x})$ the adjacency matrix of baseline subtracted signals paired with the target location $\mathbf{x}$, where the contact load is placed (see Figure S4). By this measure, symmetry violations are strongest near the boundaries of our dataset, and weakest near the center of the plate.

Throughout, heatmaps are constructed, using a 51×51 grid of pixels 5 mm on each side, as follows. For each contact load location, associated field data is attributed to the pixel that is concentric with the load in addition to all pixels completely covered by the physical extent of the contact load. We then average over all nonzero contributions to each pixel.

[a)] Electronic mail: james.l.amarel4.ctr@us.navy.mil

[b)] Electronic mail: christopher.c.rudolf.civ@us.navy.mil

II. ADDITIONAL LOCATOR VISUALIZATIONS

Expected performance can be visualized by averaging the test errors across different initializations (see Figure S5). Similarly, we also estimate model uncertainty by calculating the pointwise error variance (see Figure S6). Additionally, a heatmap of the learned equivariance error can be obtained as follows (see Figure S7). Let Ψ be a neural network designed to act on V, an adjacency matrix of signals. The mean equivariance error field is then

$$Q(\mathbf{x}) = \frac{1}{8} \sum_{g \in G} \|\rho_g \Psi[V(\mathbf{x})] - \Psi[\rho_g V(\mathbf{x})]\|. \tag{S1}$$

While there is limited similarity between the learned equivariance errors (see Figure S7) and our naive measure of input data equivariance (see Figure S4), the *approximately equivariant* model appears to learn some nontrivial structure. Evidence for this assertion lies in the fact that the *approximately equivariant* model learns symmetry-breaking weights that in the deeper layers only weakly deviate from unity (see Figure S8).

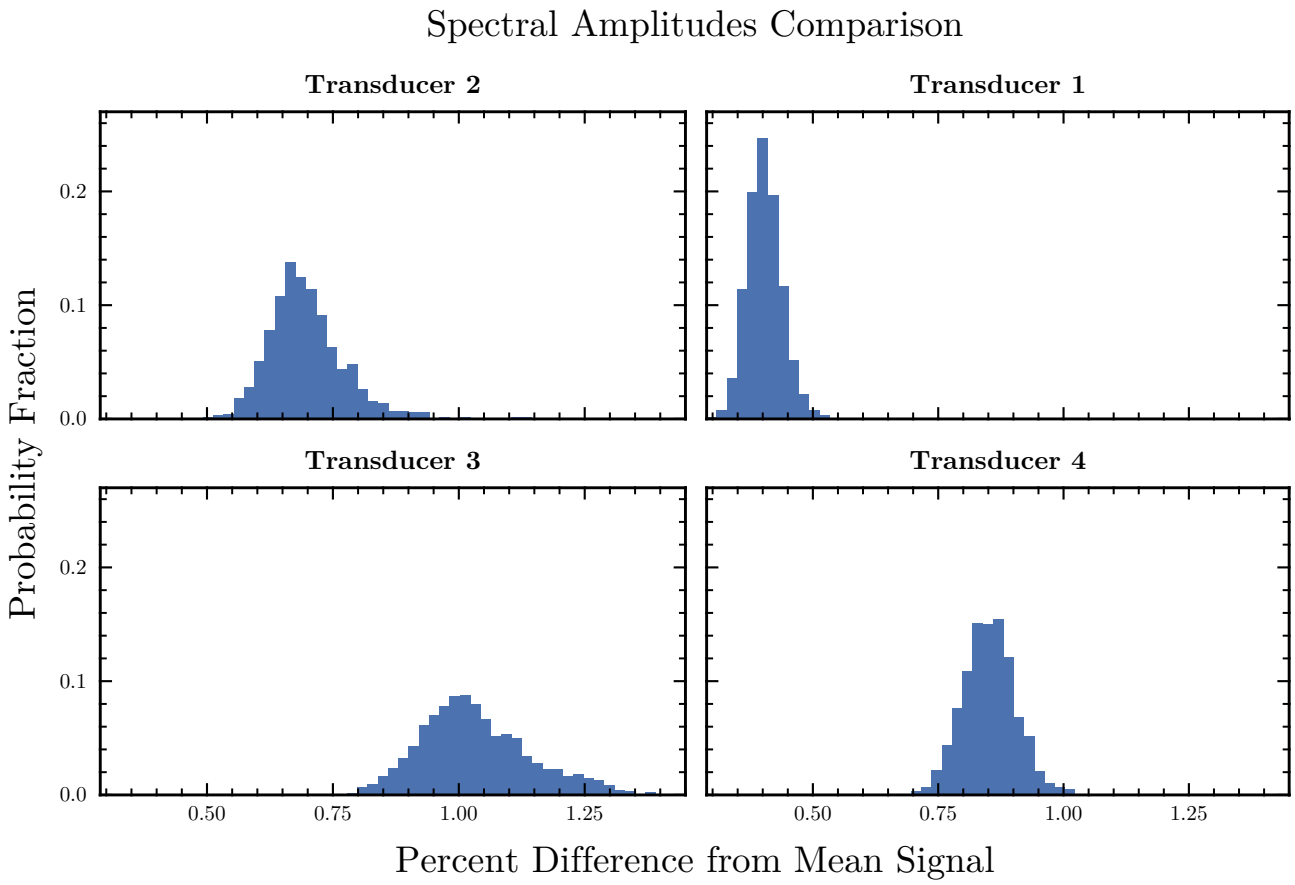

FIG. S1: Truncated histograms of the Euclidean distance between a given signal's spectral amplitude and the mean spectral amplitude. Rejected examples are not shown.

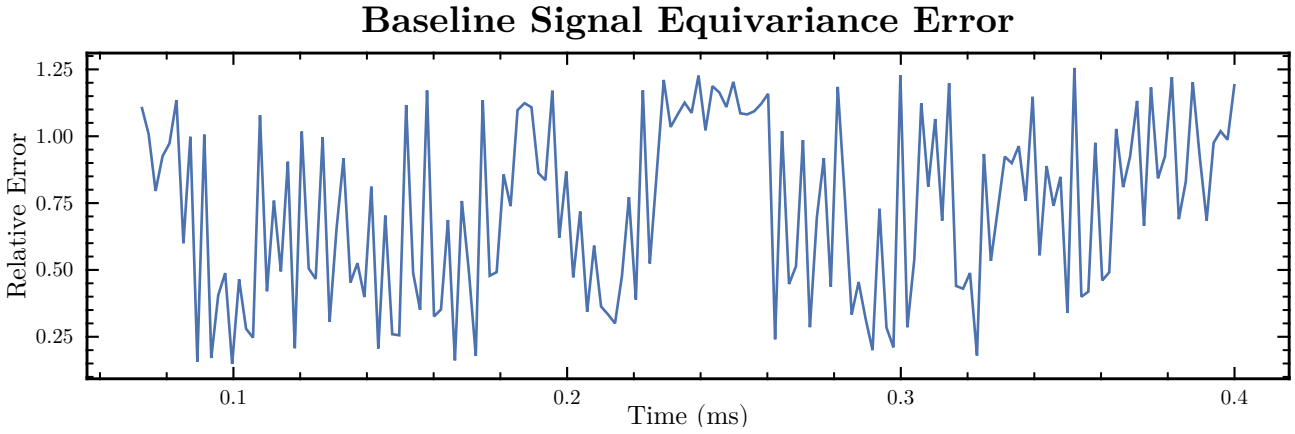

FIG. S2: Baseline received signal equivariance error.

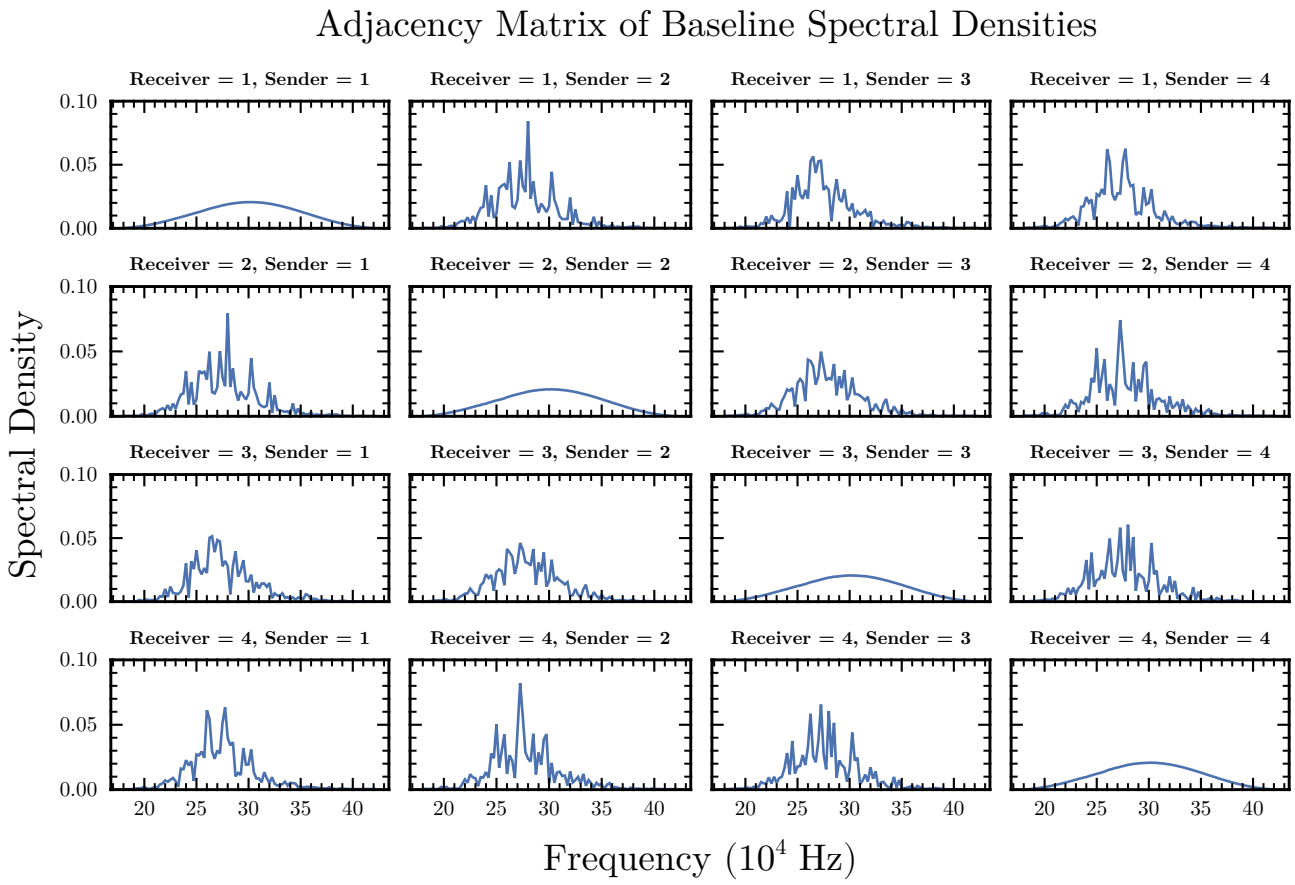

FIG. S3: Average Fourier spectral densities of the baseline signals.

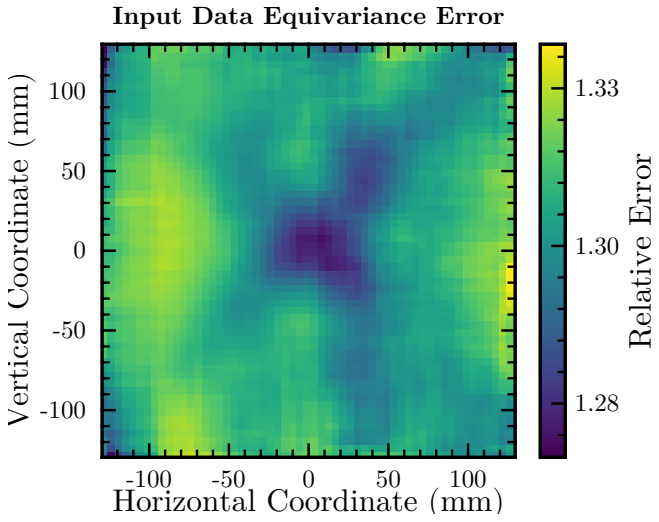

FIG. S4: Heatmap of the input data equivariance error.

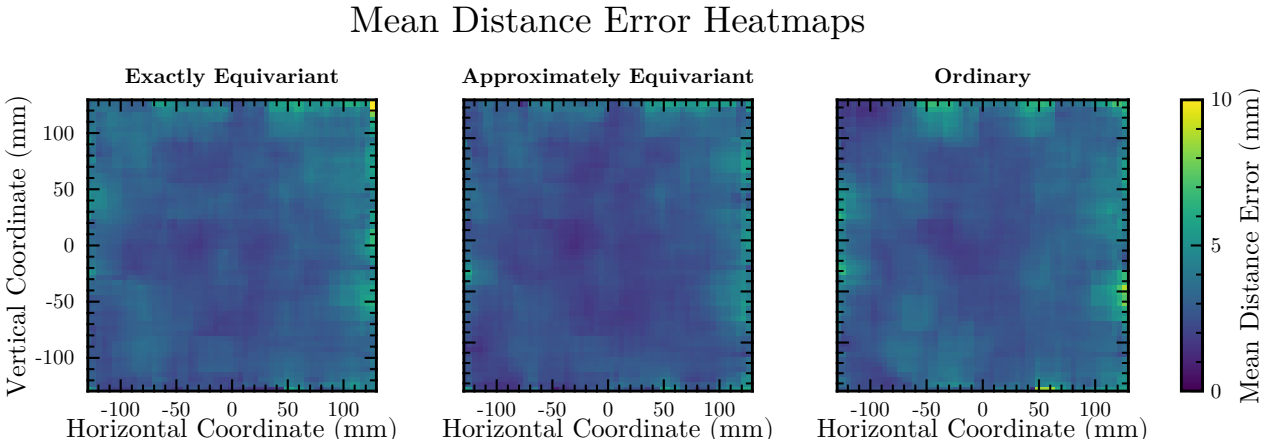

FIG. S5: Initialization averaged mean distance error heatmaps.

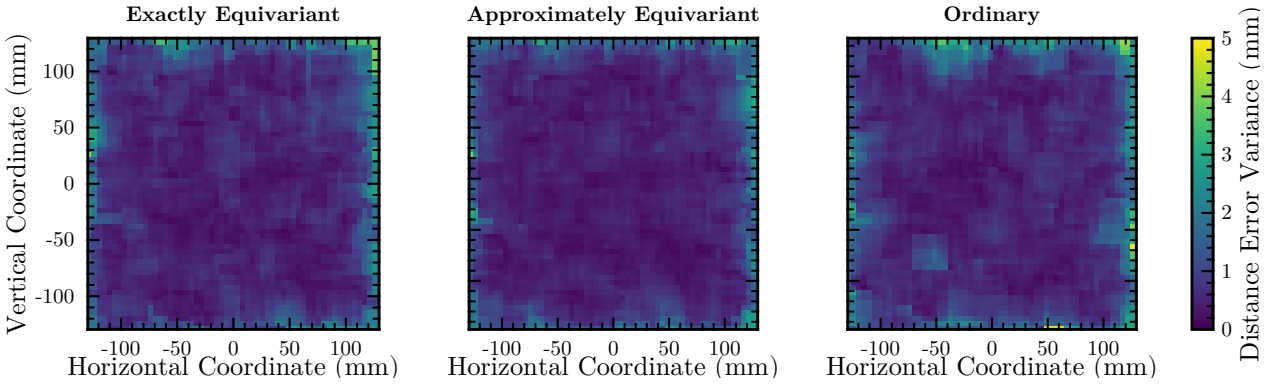

FIG. S6: Inference error variance heatmaps.

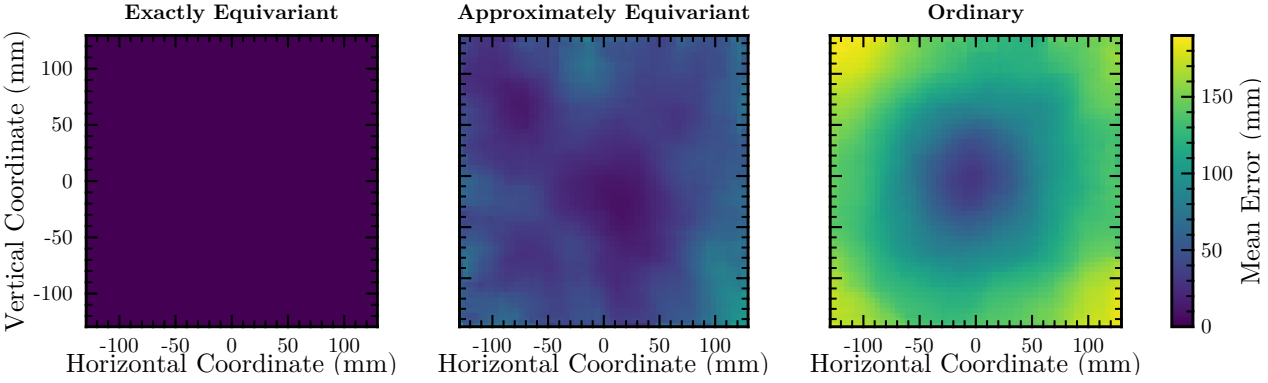

FIG. S7: Initialization averaged learned equivariance error heatmaps.

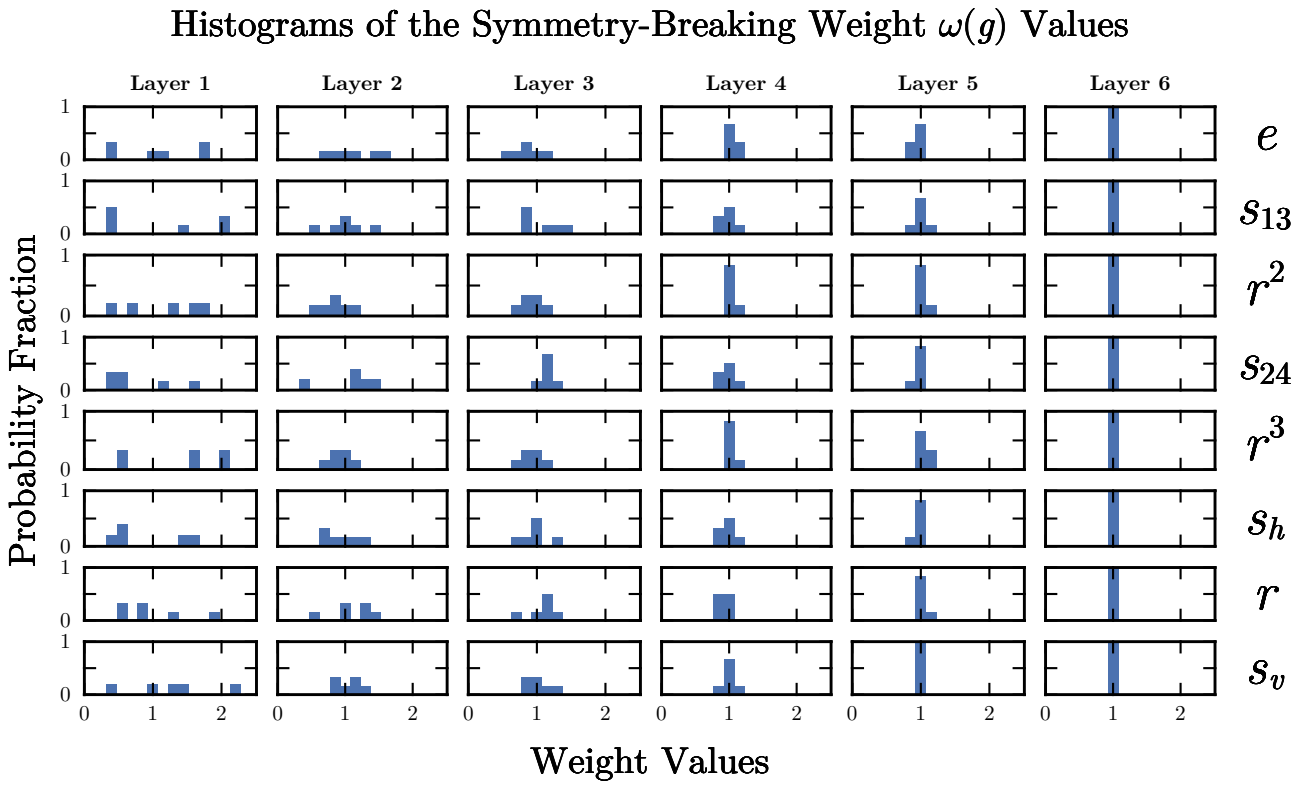

FIG. S8: Layer-wise distribution of the *approximately equivariant* model's learned symmetry-breaking weights. Here, the group elements are indicated by e for the identity element, r for a $\pi/2$ rotation, s_v for a reflection across the vertical axis, s_h for a reflection across the horizontal axis, and s_{13} and s_{24} for reflections across the diagonal connecting corner 1 with 3 and 2 with 4, respectively.